JMEPEG (2012) 21:837–848
DOI: 10.1007/s11665-011-0004-3

1059-9495/$19.00

# A Computational Investigation of the Multi-Hit Ballistic-Protection Performance of Laminated Transparent-armor Systems

*Mica Grujicic, B. Pandurangan, and N. Coutris*

*(Submitted April 25, 2011)*

**Multi-hit ballistic-protection performance of a prototypical laminated glass/polycarbonate transparent armor is investigated using a series of transient nonlinear dynamics analyses of armor impact with a sequence of four M2AP full metal jacket (FMJ) armor-piercing bullets. All calculations were carried out using ABAQUS/Explicit commercial finite element program (ABAQUS Version 6.7, User Documentation, Dessault Systems, 2007), and the computational results obtained were compared to their experimental counterparts obtained by Dolan (Ballistic Transparent-armor Testing Using a Multi-hit Rifle Pattern, Bachelors, Thesis, Kettering University, December 2007). The comparison revealed that (a) The proposed computational procedure can reasonably well account for the observed multi-hit ballistic-protection performance of the laminated transparent armor; (b) The role of prior bullet hits in reducing armor's ballistic-protection performance is clearly revealed; (c) The role of polycarbonate lamina in preventing glass fragments from entering the vehicle interior is clearly demonstrated; and (d) Experimentally observed inability of the transparent armor to defeat 0.50-caliber Fragment Simulating Projectiles (FSPs) is confirmed.**

**Keywords** ballistic performance, multi-hit capability, transparent armor

## 1. Introduction

Since the beginning of the military operations, The Operation Iraqi Freedom in Iraq and The Operation Enduring Freedom in Afghanistan, the protection and safety of the occupants of the U.S. Army ground vehicles have become an issue of critical importance. These vehicles are subjected to increased daily attacks from armed insurgents and threats from improvised explosive devices (IEDs, i.e., bombs constructed and deployed in ways different from those used in conventional military practice). Consequently, the U.S. Army is engaged in a continuing process of evaluating survivability of its vehicles and their occupants when subjected to such threats and is in a constant search for ways to improve occupant-protection capabilities and survivability of the vehicles. Considering the fact that the windows and windshields are usually the most vulnerable and the most targeted areas of the vehicle, it is understandable that these areas of the vehicle are given extra consideration.

Most transparent-armor systems currently used in the vehicle windows and windshield applications consist of stacked layers of glass and plastic (typically transparent polycarbonate, PC). Adjacent layers are bonded using interlaminate adhesives, most frequently those based on polyurethane, PUR. The outermost layer of the armor that the projectile first impacts (typically referred to as the "*strike-face*") is made of glass so that armor can efficiently deform and/or fragment the projectile. In addition, high-hardness value of glass provides the necessary resistance to scratch and abrasion which may be caused by windshield wipers, dust, etc. The back layer is typically made of polycarbonate which prevents the broken pieces of glass from entering the vehicle interior. The number of layers in a transparent-armor system, layers' thickness, as well as the total transparent-armor thickness vary from one transparent-armor system to another, as these systems are optimized with respect to their ability to protect against different types of threat (e.g., deformable or armor-piercing bullets provide different kinds of threat to the transparent armor than fragments from the IEDs).

It is well established that increased service temperatures may significantly compromise the ballistic-protection performance of transparent armor. In addition, elevated service temperatures are frequently found to cause delamination of the glass and plastic layers which seriously degrades armor transparency (a critical performance requirement for transparent-armor systems). Also lower service temperatures may induce brittleness and cracking into the inter-laminate adhesive layer giving rise to the losses in both the ballistic protection and transparency of the armor.

As mentioned above, in addition to providing the necessary level of the ballistic protection to the vehicle occupants, transparent-armor systems must also possess sufficient optical clarity/transparency. It is obvious that if no clear view of the outside is given to the vehicle occupants, they will not be able to fully carry out their duties such as drive and operate the vehicle, spot roadside mines, locate insurgent hiding places, etc. Consequently, transparent-armor systems must possess

**Mica Grujicic, B. Pandurangan,** and **N. Coutris**, Department of Mechanical Engineering, International Center for Automotive Research CU-ICAR, Clemson University, 241 Engineering Innovation Building, Clemson, SC 29634-0921. Contact e-mail: gmica@clemson.edu.

**Table 1 Ballistic performance requirements for armor as specified by the National Institute of Justice Test Standard 0108.01**

| Armor type | Test ammunition | Nominal bullet mass | Suggested barrel length | Required bullet velocity | Required hits per armor test panel | Permitted penetrations |
|---|---|---|---|---|---|---|
| I | 22LHRV | 2.6 g | 15-16.5 cm | 320 ± 12 m/s | 5 | 0 |
| | Lead | 40 gr | 6-6.5 in. | 1050 ± 40 ft/s | | |
| | 38 Special | 10.2 g | 15-16.5 cm | 259 ± 15 m/s | | |
| | R N Lead | 158 gr | 6-6.5 in | 850 ± 50 ft/s | | |
| II-A | 357 Magnum | 10.2 g | 10-12 cm | 381 ± 15 m/s | 5 | 0 |
| | JSP | 158 gr | 4-4.75 in. | 1250 ± 50 ft/s | | |
| | 9 mm | 8.0 g | 10-12 cm | 332 ± 12 m/s | | |
| | FMJ | 124 gr | 4-4.75 in. | 1090 ± 40 ft/s | | |
| II | 357 Magnum | 10.2 g | 15-16.5 cm | 425 ± 15 m/s | 5 | 0 |
| | JSP | 158 gr | 6-6.5 in. | 1395 ± 50 ft/s | | |
| | 9 mm | 8.0 g | 10-12 cm | 358 ± 12 m/s | | |
| | FMJ | 124 gr | 4-4.75 in. | 1175 ± 40 ft/s | | |
| III-A | 44 Magnum | 15.55 g | 14-16 cm | 426 ± 15 m/s | 5 | 0 |
| | Lead SWCGC | 240 gr | 5.5-6.25 in. | 1400 ± 50 ft/s | | |
| | 9 mm | 8.0 g | 24-26 cm | 426 ± 15 m/s | | |
| | FMJ | 124 gr | 9.5-10.25 in. | 1400 ± 50 ft/s | | |
| III | 7.62 mm 308 Winchester | 9.7 g | 56 cm | 838 ± 15 m/s | 5 | 0 |
| | FMJ | 150 gr | 22 in. | 2750 ± 50 ft/s | | |
| IV | 30-06 | 10.8 g | 56 cm | 868 ± 15 m/s | 1 | 0 |
| | AP | 166 gr | 22 in. | 2850 ± 50 ft/s | | |

AP, armor piercing; FMJ, full metal jacket; JSP, jacketed soft point; LRHV, long rifle high velocity; RN, round nose; SWCGC, semi-wadcutter gas checked

adequate level of optical transparency both in the visible and the infrared ranges of the electromagnetic spectrum. The latter is critical for the vehicle occupants using night-vision goggles.

As discussed above, the U.S. Army vehicles used in the current operations face two main threats: (a) attacks by the armed insurgents, and (b) explosions by the IEDs. The armed insurgents present the so-called small-arms fire threats since they are usually equipped with handguns, small caliber rifles, or medium machine guns. The small-arms projectiles come in sizes between 9 and 12.7 mm and in different types (e.g., ball ammunition, armor-piercing rounds, tracers, etc.). The IED threats are more difficult to describe and quantify. Currently, when testing armor's ballistic-protection capability against the IED threats, the so-called Fragment Simulating Projectiles (FSPs) are typically used. The FSPs are generally in the shape of a right-circular solid cylinder, made of steel, and were originally introduced to model the fragments generated by exploding artillery shells.

To ensure that its vehicles are combat ready, the U.S. Army requires their regular testing for ballistic-protection performance. Also, new vehicles are being designed with improved protection capabilities. However, the new vehicles must also have significantly reduced weight (to ensure their high mobility, rapid deploying ability, high fuel efficiency, etc.). Since the transparent-armor systems are one of the weakest areas on the vehicle and provide the most inefficient weight-normalized ballistic protection, they present the vehicle designers with significant challenges. Consequently, successful design of the future military ground vehicles entails a complete understanding of the ballistic-protection performance of the competing transparent-armor systems under different threats. In particular, knowledge of the ability of armor to provide multi-hit ballistic protection without significant loss in its optical transparency under different threats is important.

In its current practice for acquiring the transparent armor, the U.S. Army uses the ballistic-performance specifications for commercially available armor like the ones mandated by the National Institute of Justice Test Standard 0108.01, Table 1. The specifications listed in Table 1 define, for different threat levels (I, II, II-A, III, III-A, and IV), projectiles' type, weight, velocity, barrel length, and allowable number of penetrations for a given number of hits per armor test panel. As discussed earlier, current ballistic threats far exceed the ones considered in commercial transparent-armor ballistic-performance specifications. That is, these specifications typically cover only protection requirements against handguns and small-caliber rifle rounds, while the U.S. Army vehicles face threats from a larger range of heavier ammunition. Consequently, the U.S. Army is developing a new transparent-armor purchase document ATPD 2352 which outlines all of the new key requirements for the transparent-armor systems and which will guide future armor acquisition by the Army. In addition to specifying the ballistic-protection requirements with respect to the standard military threats (bullets of various shapes and sizes), the ATPD 2352 also includes the ballistic-performance requirements with respect to the FSPs as well as the optical transparency and environmental durability requirements. The inclusion of the armor-protection requirements against the FSP threats is particularly critical considering the fact that IED-related vehicle occupant deaths are on the rise.

While most details pertaining to a threat level, the testing procedures and the required test results for transparent-armor systems qualification are classified, a rendition of these specifications was used in the recent study by Dolan (Ref 1),

who carried out a detailed experimental investigation of the ballistic-protection performance of a laminated glass/polycarbonate transparent-armor system subjected to a rifle-round multi-hit threat. The study of Dolan clearly revealed numerous experimental challenges and excessive cost associated with experimental investigations of the ballistic-protection performance of complex transparent-armor systems. Consequently, any use of computational engineering analyses, which would reduce the need for experimental testing and speed up the development of new transparent-armor systems with superior multi-hit ballistic-protection performance is attractive. In the present study, a series of transient nonlinear dynamic simulations of a prototypical laminated glass/polycarbonate transparent-armor system when subjected to a multi-hit threat from the M2AP rifle-fired armor-piercing bullet is carried out to examine the utility of such analysis. Toward that end, the computational results are compared with their experimental counterparts obtained in the study of Dolan (Ref 1).

The organization of the article is as follows: In section 2.1, a brief overview is provided of the experimental set-up and procedures used, and the results obtained in the study of Dolan (Ref 1) who carried out an assessment of the multi-hit ballistic performance of transparent armor. Details regarding the corresponding transient nonlinear dynamics computational analysis as well as regarding the material models used are presented in section 2.2. The main results obtained in the present study are presented and discussed in section 3. The key conclusions drawn from the present study are summarized in section 4.

## 2. Experimental and Computational Procedures

### 2.1 Experimental Investigation

In this section, a brief description is provided of the experimental procedures and the results obtained in the recent ballistic-testing study of Dolan (Ref 1) which was carried out at the TARDEC Armor Integration Laboratory (TAIL) located on the TARDEC army base in Warren, MI. Within the experimental procedure used, plate-like laminated glass/polycarbonate transparent-armor test panels were mounted vertically in a specially designed test fixture which ensures consistent and reproducible test-panel clamping conditions. Test-panel dimensions were $L \times W \times T = 304.8$ mm $\times$ 304.8 mm $\times$ 73 mm, and each panel consisted of five 10.42-mm-thick glass layers and five 4.17-mm-thick polycarbonate layers. In accordance with the laminated glass/polycarbonate transparent-armor installation procedures on a vehicle, the glass face of the armor test panels is considered as the strike face. A 0.3-caliber M2AP armor-piercing rifle-fired bullet rounds were used velocity of which was determined using a customized chronographic system placed in front of the installed test panels. Each transparent-armor test panel was impacted with four M2AP rounds, and the multi-hit test pattern used is displayed in Fig. 1. A 0.508-mm-thick aluminum foil, placed parallel to and 150 mm behind the fixtured test panel, was used as a witness plate. While, during testing of the common opaque armor, a thicker witness plate is used to mimic the uniform and skin of a soldier, in the present case, a thinner witness plate is used which acts as a surrogate for the soldiers' eye cornea. Hence, any perforation of the witness plate signifies a potential eye injury for the soldiers not wearing any eye protection and is considered as failure ("complete penetration") of the tested transparent-armor system. Any other outcome of the armor testing qualifies as a "partial penetration."

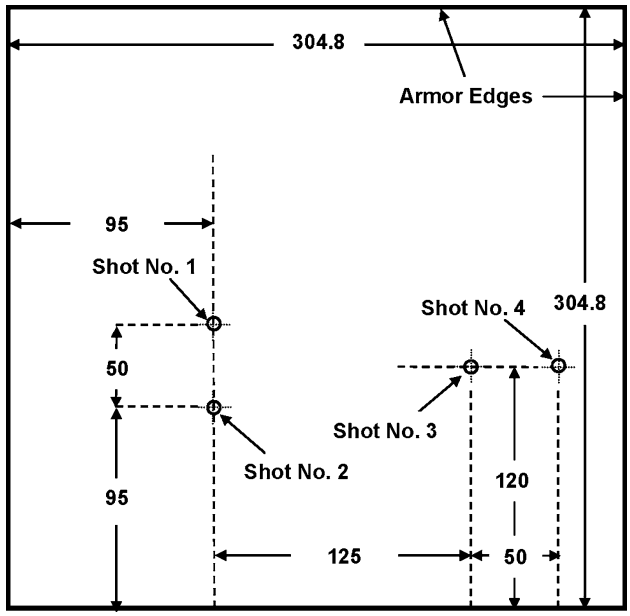


**Fig. 1** Impact locations and firing sequence for the multi-hit ballistic-performance test analyzed in the study of Dolan (Ref 1) and in the present study. All dimensions are in mm

It is customary to quantify the ballistic-protection performance of the opaque armor with respect to a given threat using $V_{50}$, i.e., average projectile velocity at which the probability of armor penetration is 50%. When single-hit ballistic performance of the armor is tested, one impact is made into each virgin armor test panel, or several well-spaced hits are made into a single virgin armor test panel. Each impact involves the same type of projectile at an increased incident velocity. Each impact is considered to be a separate statistical event and, consequently, $V_{50}$ is obtained by the so-called "six-round limit" procedure in which the average single-hit $V_{50}$ is computed among the three highest velocities at which partial penetrations take place and the three lowest velocities at which complete penetrations take place.

When multi-hit ballistic-protection performance of armor is tested, the entire set (four in the present case) of hits associated with a given average projectile velocity are considered as a single statistical event since closely spaced hits affect ballistic response of the armor. Hence, if any of the four hits results in a complete penetration of the armor, the entire set of four hits is considered to lead to a failure of the armor system. Typically, as the average projectile velocity is increased from the lower values, at which only partial penetrations take place, to the higher values, at which complete penetrations take place, a "zone of mixed results" is encountered. Within this zone, complete penetrations take place at lower projectile velocities and partial penetrations take place at higher projectile velocities. The multi-hit $V_{50}$ is then calculated using only the armor testing results in the zone of mixed results, i.e., to get the multi-hit $V_{50}$, the sum of all average projectile velocities in the zone of mixed results is divided by the number of multi-hit tests lying in this zone.

Considering high vulnerability of transparent armor, its ballistic-protection performance is typically quantified not by $V_{50}$, but by the highest average velocity of the given projectile at which the probability for complete penetration is 5% or less. To determine this velocity (referred to in the remainder of the manuscript as, $V_{05}$), and considering the fact that the outcome of each multi-hit test could be either complete penetration or partial penetration, one must use the logistic regression analysis to construct the corresponding logistic regression curve which relates the probability for complete penetration of the armor, $P$, with the average projectile velocity, $v$. This curve is defined by the following functional relationship:

$$P = \frac{\exp(\beta_0 + \beta_1 v)}{1 + \exp(\beta_0 + \beta_1 v)} \quad \text{(Eq 1)}$$

where $\beta_0$ and $\beta_1$ are regression coefficients. To evaluate these coefficients, the average projectile velocities (one for a given set of four hits) are grouped and, within each group, the probability of complete penetration of the armor determined by dividing the number of tests resulting in full penetration by the number of tests in that projectile-velocity group. Once the procedure is completed, Eq 1 is linearized as

$$\ln\left(\frac{P}{1-P}\right) = \beta_0 + \beta_1 v \quad \text{(Eq 2)}$$

and the coefficients $\beta_0$ and $\beta_1$ are determined using the standard least-squares-based linear-regression (curve-fitting) analysis.

An example of the test results obtained in the experimental study of Dolan (Ref 1) is displayed in Table 2. In Table 2, the results of eleven multi-hit ballistic-protection tests each involving four shots with the location and firing sequence in accordance with Fig. 1, are displayed. For each test, an average projectile velocity and the observed (partial or complete) penetration mode are specified. The corresponding curve for probability for complete penetration of the armor, $P$, versus the average projectile velocity, $v$, obtained using the logistic regression analysis is displayed in Fig. 2.

A schematic of the typical results pertaining to a post-mortem analysis of the extent of armor damage around each of the four points of impact at the strike face of the armor obtained in the study of Dolan (Ref 1) is displayed in Fig. 3. It is seen that a zone of damage several times larger than the penetration-hole size surrounds each of the four points of impact.

**Table 2 Experimental results obtained by Dolan (Ref 1) and the computational results obtained in the present study pertaining to the multi-hit ballistic protection performance of a laminated glass/polycarbonate transparent-armor system**

| Sample number | Average projectile velocity, m/s | Penetration type Dolan (Ref 1) | Penetration type present study |
|---|---|---|---|
| 1 | 592 | Partial | Partial |
| 2 | 640 | Partial | Partial |
| 3 | 682 | Partial | Partial |
| 4 | 713 | Complete | Partial |
| 5 | 779 | Partial | Partial |
| 6 | 804 | Complete | Partial |
| 7 | 807 | Complete | Partial |
| 8 | 815 | Partial | Partial |
| 9 | 847 | Complete | Complete |
| 10 | 858 | Complete | Complete |
| 11 | 893 | Complete | Complete |

## 2.2 Computational Analysis

**2.2.1 Problem Definition.** In this section, a detailed description is provided of the geometrical models for the laminated glass/polycarbonate transparent-armor plates and the 0.3 caliber M2AP armor-piercing rounds and of the computational procedure used in a transient nonlinear dynamics analysis of the multi-hit ballistic-performance of transparent-armor samples tested experimentally by Dolan (Ref 1).

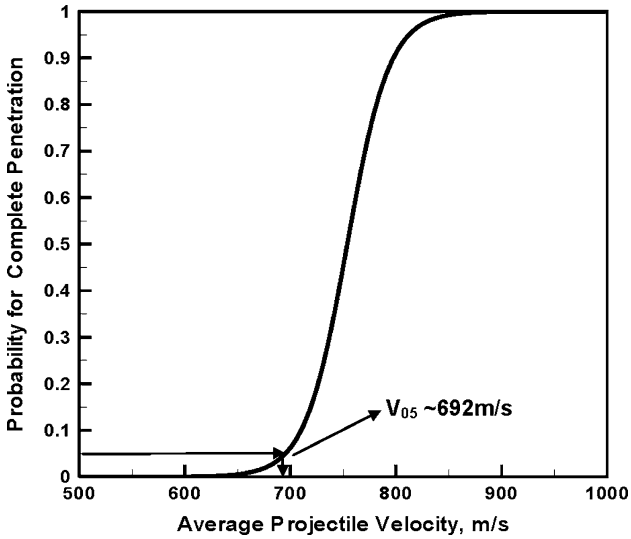


**Fig. 2** The probability for complete penetration of the armor, $P$, versus the average projectile velocity, $v$, curve obtained using the logistic regression analysis and the results of Dolan (Ref 1)

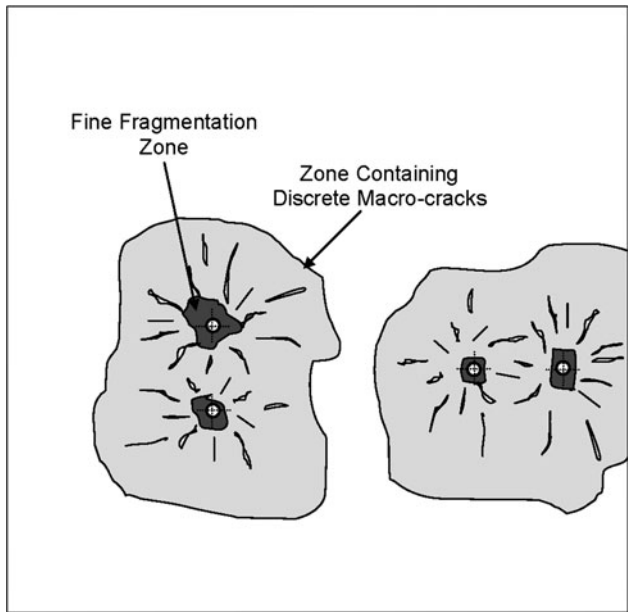


**Fig. 3** A schematic of the typical results pertaining to the damage zone size surrounding each of the four points of impact of the transparent armor as observed in the study of Dolan (Ref 1) on the strike face of the armor

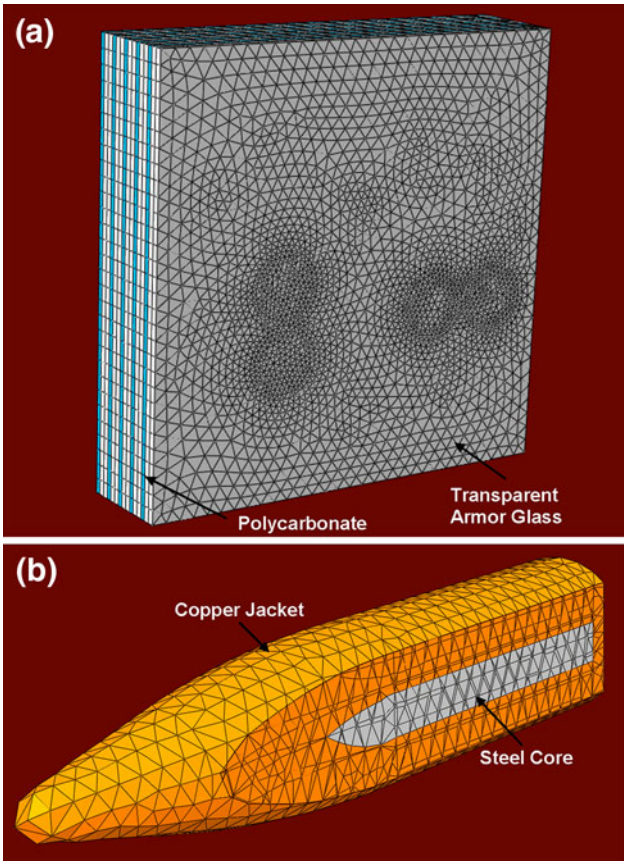


**Fig. 4** Typical finite element meshes used for discretization of (a) transparent-armor test sample and (b) projectile

A schematic of the transparent-armor square-plate like test sample analyzed is depicted in Fig. 4(a). It consists of five alternating 10.42-mm-thick soda-lime glass laminae and five 4.17-mm-thick polycarbonate laminae, making the overall test-sample thickness of 73 mm. The in-plane ($y$-$z$) dimensions of the sample are 304.8 mm × 304.8 mm. Both the glass and the polycarbonate laminae are meshed using solid six-node reduced-integration (C3D6R) elements. A finer mesh was used in the region of the armor surrounding the four points of impact where the elements' average edge length was ~4 mm. Typically, there were 8680 elements in a single layer of glass and 4340 elements per layer of polycarbonate. The inter-lamina polyurethane adhesive was not modeled explicitly. Instead, a single layer of six-node cohesive elements (COH3D6) is introduced between the contacting glass and polycarbonate laminae and the tensile and shear strength of polyurethane used to derive the corresponding normal and shear cohesive properties of these elements.

The 0.3-caliber conical pointed-tip M2AP round is 35.6 mm long and consists of a 1-mm-thick copper jacket and a hard AISI 4340 steel core. The weight of the projectile is ~10.75 g. A schematic of the M2AP round is depicted in Fig. 4(b). The copper jacket and the AISI 4340 steel core are meshed using 4048 and 3220 four-noded tetrahedron (C3D4R) elements, respectively, with an average element edge length of 1 mm. The jacket and the core share nodes along their contact surface, i.e., a perfect jacket/core interfacial bonding is assumed.

The mesh sizes both for the transparent-armor test-sample and the projectile were varied initially to validate that the computational results are not significantly mesh-size dependent.

All the calculations were carried out using ABAQUS/Explicit computer program (Ref 2). Built-in material models were used for all materials except for glass which was represented using the material model recently proposed by Grujicic et al. (Ref 3-8). This model was implemented into a *VUMAT* User Material Subroutine and linked with ABAQUS/Explicit before the model could be used.

Interactions between the projectile and armor were modeled using the "Hard Contact Pair" type of contact algorithm. Within this algorithm, contact pressures between two bodies are not transmitted unless the nodes on the "slave surface" contact the "master surface." No penetration/over-closure is allowed, and there is no limit to the magnitude of the contact pressure that could be transmitted when the surfaces are in contact. Transmission of shear stresses across the contact interfaces is defined in terms of a static, $\mu_{st}$, and a kinematic $\mu_{kin}$, friction coefficient, and an upper-bound shear stress limit, $\tau_{slip}$ (the maximum value of shear stress which can be transmitted before the contacting surfaces begin to slide).

The impact of the projectile with armor is modeled by assigning an initial (translational) velocity to the projectiles ("the initial condition"). To model sequential impact of the four projectiles, the projectiles were positioned at different distances from the armor and propelled at the same velocities at the same time. The initial velocity of armor was set to zero and, during the impact simulation, the narrow side, the top, and bottom faces of the target normal to the impacted face was kept at a fixed position ("the boundary conditions").

To prevent hour-glassing effects which may arise because of the use of reduced-integration elements, a default value of hour-glass stiffness was used. No mass-scaling algorithm was used to increase the maximum stable time increment. Computational analyses were run on a machine with two 2.33 GHz Quad-core Intel Xeon processors with 16 GB of RAM. A typical 1-ms impactor/target computational analysis would require 5 h and 30 min of (wall-clock) time.

An example of the initial configuration and an intermediate configuration for the finite element model involving four bullets, a laminated transparent-armor panel and a thin-wall witness-plate is displayed in Fig. 5(a) and (b), respectively.

**2.2.2 Material Models.** As mentioned in the previous section, the transparent-armor samples consist of three materials: soda-lime glass, polycarbonate, and a polyurethane adhesive. Also, the M2AP rounds consist of a copper jacket and an AISI 4340 steel core. Considering the fact that the M2AP round was used in our recent study (Ref 9), and that the material models (a linear equation of state, the Johnson-Cook strength model, the Johnson-Cook failure model, and an erosion algorithm based on the maximum allowable instantaneous geometrical strain) used for copper and AISI 4340 steel were reviewed in great detail in that study (Ref 9), no further discussions of the material models for copper and AISI 4340 steel will be given here. Glass, polycarbonate, and polyurethane adhesive, on the other hand, are the key material constituents in the laminated transparent-armor and material models, which are used for accounting for their mechanical response under large-strain, high deformation rate, high-pressure conditions, etc. encountered during impact with a high-speed projectile, are presented in the remainder of this section.

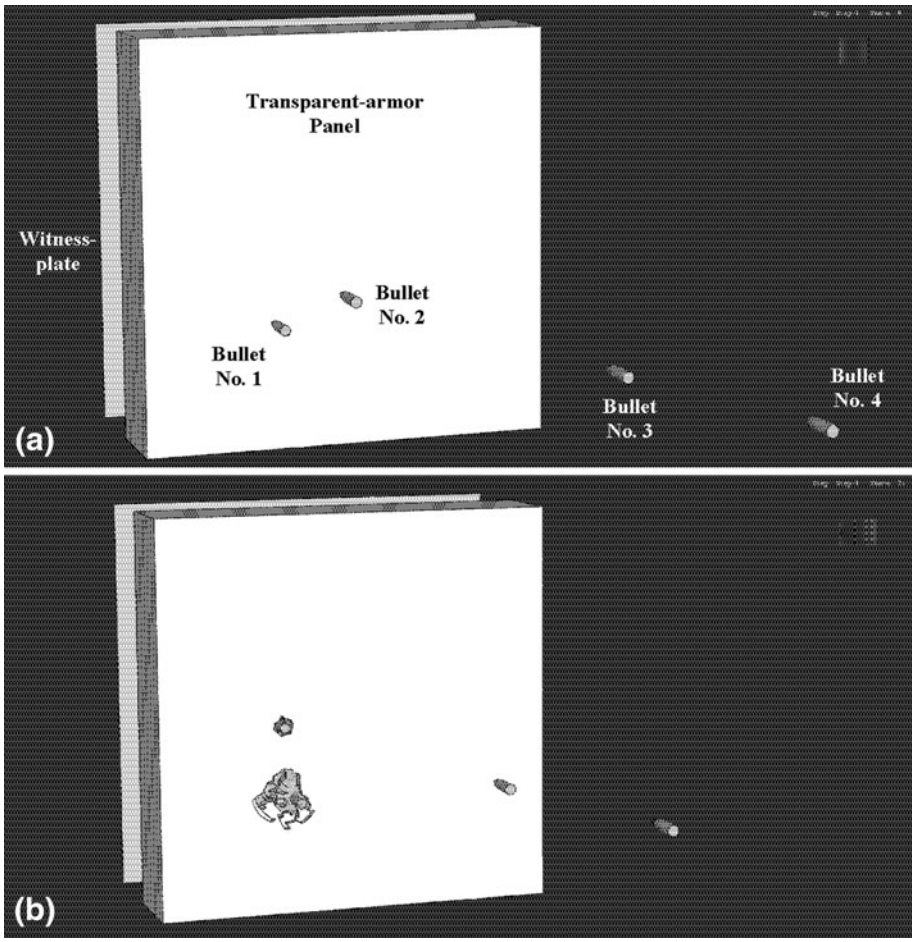


**Fig. 5** An example of (a) the initial configuration and (b) an intermediate configuration of the projectiles/armor/witness-plate system analyzed in the present study

*Soda-Lime Glass.* As mentioned above, mechanical behavior of the soda-lime glass laminae in the armor is represented using our recent model (Ref 3-8). In the remainder of this subsection, a brief overview of the model is provided.

The model of Grujicic et al. (Ref 3-8) is physically based and treats glass as a stochastic brittle material whose damage-dominated deformation and ultimate failure are controlled by the pre-existing flaws. To account for the potential role of glass-panel processing and handling, different distributions of flaws are assumed for the surface and bulk regions of the material. The key feature of the model is that it enables glass, depending on the loading conditions, to fail in either a coarse-fragmentation or a fine-fragmentation/comminution mode. The two modes of failure are the result of competition of the following two basic processes:

(a) The growth of newly nucleated cracks which is accompanied by the growth of "*shielding*" zones, one zone surrounding each crack. Within the zones the pre-existing flaws are shielded from the external field and can not be activated and converted into cracks. This, in turn, leads to the course-fragmentation mode of failure; and
(b) An increase in the stress-level in the regions surrounding shielding zones of the newly nucleated cracks which promotes nucleation of additional cracks. The resulting nucleation of multiple cracks causes the cessation of their growth, a gradual degradation of the materials' mechanical properties and, ultimate, multiple fine-scale fragmentation.

In the model, coarse-fragmentation fracture mode is promoted by low-strain rates while high-strain rates lead to the fine-fragmentation mode (comminution). A critical deformation rate is defined, which separates the two fracture modes. The model was fully validated by comparing the model-based prediction of a computational analysis of the so-called Edge-on-Impact (EOI) test with the experimental results obtained in the study of Strassburger et al. (Ref 10).

Finite element implementation of the model is carried out using the following procedure:

(a) When a finite element is failing in the *coarse-fragmentation mode*, a single crack is assumed to extend, at the terminal velocity, through the element. The total time for element failure is obtained by dividing the characteristic element dimension by the terminal crack velocity. Once the element has fractured, it is removed from the model. In other words, multi-axial macro-cracking is not handled explicitly. When an element is undergoing coarse-fragmentation failure, stiffness and strength properties of this element are degraded linearly with the corresponding crack strain from the point of crack initiation to the point of complete traversal of the element by the crack;

(b) When an element has started undergoing *multi-fragmentation damage* because of the formation of multiple cracks, stress-shielding and path-crossing effects initially prevent the nucleation of macro-cracks. However, when the extent of *coherent damage* within a single element reaches a *critical value*, this element is assumed to fracture by micro-crack coalescence and to lose most of its ability to support load. To account for the experimental observations that the resulting micro-fragments remain confined by the surrounding non-fractured material and can support compressive and shear loads, the elements that failed in the multi-fragmentation mode are not removed from the model. Instead, they are retained and assigned small residual normal and shear stiffness values; and

(c) When an element is experiencing *multiple-fragmentation damage*, the extent of damage, $D$, is governed by a damage evolution equation and the degradation of the corresponding stiffness and stress properties of the material are governed by the appropriate damage-dependent stiffness and strength relations.

Thus, the key components of the soda-lime glass model proposed by Grujicic et al. (Ref 3-8) are (i) the Weibull-type surface and bulk flaw distribution parameters; (ii) a coarse-fragmentation/fine-fragmentation threshold stress rate; (iii) a damage evolution equation; and (iv) damage-induced stiffness and strength degradation equations. To couple the model with the ABAQUS/Explicit computer program (Ref 2), it had to be implemented into a *VUMAT* User Material Subroutine.

*Polycarbonate.* While polycarbonate in its rubbery/leathery state above the glass transition temperature and under low strain-rate loading conditions can have considerable ductility and a quite complex mechanical response, the same material when subjected to high strain rates behaves essentially as a rate-independent isotropic linear elastic and rate-dependent isotropic ideal plastic material with plastic strain-controlled failure (Ref 11). Since in the present study, polycarbonate laminae were subjected to high deformation rates, this simple material model for polycarbonate was used. A list of material model parameters for the polycarbonate is given in Table 3.

*Polyurethane Adhesive.* The polyurethane adhesive used to bond adjacent glass and polycarbonate laminae is not modeled as a conventional structural hyper-elastic material. Instead this material was modeled in the present study using the "*cohesive zone framework*" originally proposed by Needleman (Ref 12). The cohesive zone is assumed to have a negligible thickness

**Table 3 Rate-independent isotropic linear elastic, rate-dependent isotropic ideal plastic and plastic strain-based failure material model parameters for polycarbonate (Ref 11)**

| Parameter | Units | Value | Strain rate, $s^{-1}$ |
|---|---|---|---|
| Young's modulus | GPa | 2.5 | N/A |
| Poisson's ratio | N/A | 0.24 | N/A |
| Yield strength | MPa | 45 | 400 |
| Yield strength | MPa | 50 | 1700 |
| Yield strength | MPa | 70 | 2200 |
| Failure plastic strain | N/A | 2.0 | N/A |

when compared with other characteristic lengths of the problem, such as the glass/polycarbonate lamina thickness and the characteristic lengths associated with the stress/strain gradients. The mechanical behavior of the cohesive zone is characterized by a traction-displacement relation, which is introduced through the definition of an *interfacial potential*, $\psi$. The perfectly bonded glass/polycarbonate interface is assumed to be in a stable equilibrium, in which case the potential $\psi$ has a minimum and all tractions vanish. For any other configuration, the value of the potential is taken to depend only on the normal, $U_n$, and tangential displacements discontinuities (jumps), $U_t$, across the interface. The interface potential of the following form initially proposed by Socrate (Ref 13) is used in the present study:

$$\psi(U_n, U_t) = \left\{-e\sigma_{max}\delta_n + \frac{1}{2}\tau_{max}\delta_t \log\left[\cosh\left(2\frac{U_t}{\delta_t}\right)\right]\right\}\left[e^{-\frac{U_n}{\delta_n}}\left(1+\frac{U_n}{\delta_n}\right)\right] \quad \text{(Eq 3)}$$

where the parameters $\sigma_{max}$ and $\tau_{max}$ are, respectively, the normal and tangential interfacial (cohesion) strengths, and $\delta_n$ and $\delta_t$ are the corresponding characteristic interface (separation/sliding) lengths. Differentiation of Eq 3 with respect to $U_n$ and $U_t$ yields the following expressions for the normal and tangential interfacial tractions:

$$F_n(U_n, U_t) = \left\{e\sigma_{max} - \frac{1}{2}\tau_{max}\frac{\delta_t}{\delta_n}\log\left[\cosh\left(2\frac{U_t}{\delta_t}\right)\right]\right\}\left[\frac{U_n}{\delta_n}e^{-\frac{U_n}{\delta_n}}\right] \quad \text{(Eq 4)}$$

$$F_t(U_n, U_t) = \left[\tau_{max}\tanh\left(2\frac{U_t}{\delta_t}\right)\right]\left[e^{-\frac{U_n}{\delta_n}}\left(1+\frac{U_n}{\delta_n}\right)\right] \quad \text{(Eq 5)}$$

Graphical representations of the two functions defined by Eq 4 and 5 are given in Fig. 6(a) and (b), respectively. If $F_n$ given by Eq 4, is expressed for the case of purely normal interface decohesion, and the $F_t$ for the case of pure sliding, one obtains:

$$F_n(U_n, U_t = 0) = F_n^o(U_n) = e\sigma_{max}\left(\frac{U_n}{\delta_n}e^{-\frac{U_n}{\delta_n}}\right) \quad \text{(Eq 6)}$$

$$F_t(U_n = 0, U_t) = F_t^o(U_t) = \tau_{max}\tanh\left(2\frac{U_t}{\delta_t}\right) \quad \text{(Eq 7)}$$

An inspection of Eq 6 and 7 shows that the glass/polycarbonate interface behavior is characterized by four parameters: $\sigma_{max}$, $\delta_n$, $\tau_{max}$, and $\delta_t$; where $\sigma_{max}$ is the peak normal traction for purely normal interface decohesion (i.e., the normal decohesion strength); $\delta_n$ is the normal interface separation which corresponds to this peak traction; $\tau_{max}$ is an asymptotic shear traction for interface sliding (i.e., the shear decohesion strength); and $\delta_t$ is a characteristic length in pure sliding, which corresponds to a shear traction 1% lower than $\tau_{max}$,. i.e., $F_t^o(\delta_t) \approx 0.99\tau_{max}$. For the case of polyurethane bonded glass/polycarbonate interfaces, these four parameters were determined in our previous study (Ref 14).

## 3. Results and Discussion

In section 2.2, a detailed description was provided regarding the transient nonlinear dynamics finite element analyses of the

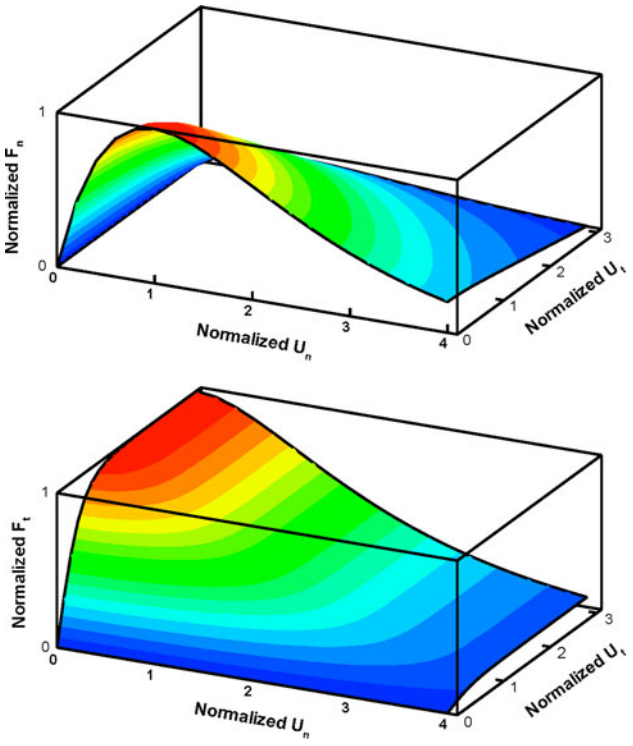


**Fig. 6** Normalized normal, $F_n$, and tangential components, $F_t$, of the traction per unit interface area, as a function of the normalized normal, $U_n$, and normalized tangential, $U_t$, components of the interface displacements

multi-hit ballistic protection tests of a prototypical laminated transparent-armor system. In the present section, the main results of the multi-hit ballistic protection computational analyses are presented and discussed.

### 3.1 Multi-Hit Ballistic Performance of the Transparent-armor System

To validate the present multi-hit ballistic performance computational analyses, the analyses were carried out at the same initial velocities of the M2AP full metal jacket (FMJ) armor-piercing bullets as those used in the study of Dolan (Ref 1), Table 2. The results of these analyses are listed in the last column of Table 2. It is seen that for the most part the experimental and the computational results are in full agreement. However, the computational analyses carried out did not reveal the presence of the zone of mixed results. One possible explanation for this apparent discrepancy is the fact that the same initial population of pre-existing flaws was assumed in all the computational analyses carried out in the present study. In the experimental study of Dolan (Ref 1), on the other hand, each multi-hit ballistic-protection test was carried out using a different laminated transparent-armor panel. Owing to the statistical nature of the size and potency of pre-existing flaws, each of the test panels used in the study of Dolan (Ref 1) is expected to have comprised different populations of the flaws. Our preliminary investigation has shown that the zone of the mixed results could be obtained if different initial populations of the flaws are taken in the analyses of ballistic-protection performance of the transparent-armor test panels at different projectile velocities. However, to fully account for the effect of variations in the initial population of the pre-existing flaws, a more rigorous statistical procedure should be employed to analyze the obtained computational results. Such analysis was beyond the scope of the present study.

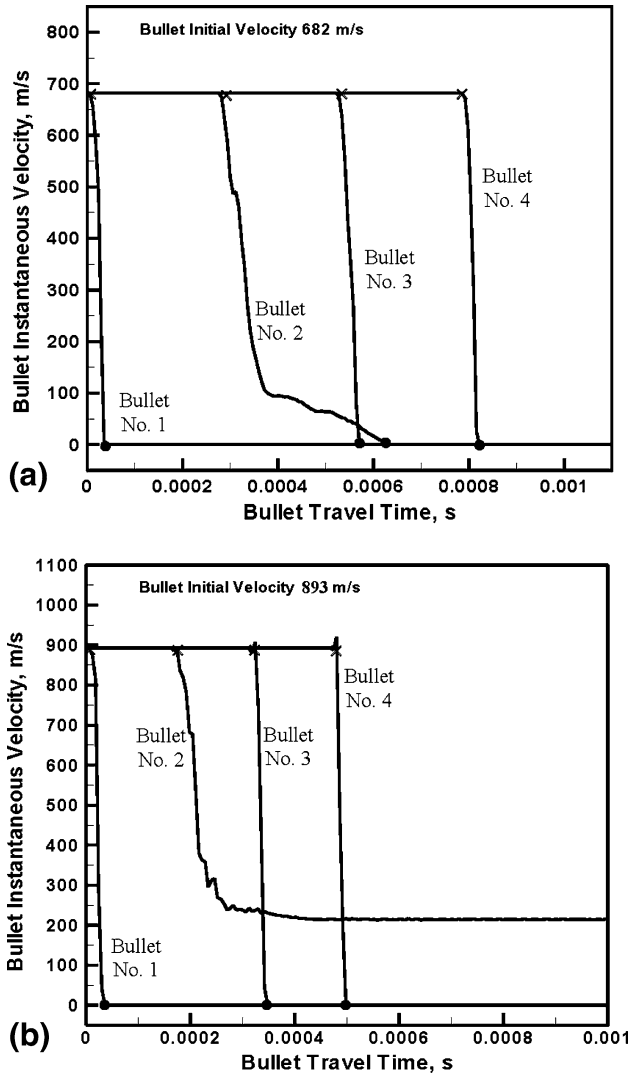


**Fig. 7** Temporal evolutions of the velocity of four M2AP projectiles during their impact with the laminated transparent-armor system for the initial projectile velocities of (a) 682 m/s and (b) 893 m/s

### 3.2 Temporal Evolution of the Bullets' Velocity

In order to better understand the multi-hit ballistic-protection performance of the transparent-armor samples investigated in the present study, the temporal evolutions of the velocity for each of the four M2AP FMJ armor-piercing bullets are recorded and analyzed. An example of the results pertaining to the temporal evolutions of the velocities of the four projectiles in the case of the initial bullet velocity of 682 m/s (the highest velocity at which partial penetration of the armor was observed in the study of Dolan; Ref 1) are displayed in Fig. 7(a). For each of the four bullets, an "X" is used to denote the moment when the bullet first makes contact with the armor, whereas a "•" is used to denote the instant of bullet arrest. To quantify the multi-hit ballistic performance of the armor in this case (partial-penetration case), the time periods between the bullet/armor first contact and the bullet arrest are recorded for all the four

bullets as follows: bullet 1—35 μs, bullet 2—320 μs, bullet 3—37 μs, and bullet 4—39 μs. These results clearly reveal that the ability of the armor to defeat the projectile is compromised by the prior impact of the armor by the projectile(s). In addition, the effect of higher local levels of failure strength (associated with the current population of flaws), and the proximity of the lateral confinement induced by the clamped edges of the test panels is also revealed. Consequently, it takes the (undamaged) armor 35 μs to stop the first bullet, while the same armor after suffering damage because of the impacts of bullets 1-3 takes 39 μs to stop the fourth bullet. On the other hand, higher levels of failure strength and the proximity of the right-clamped edge to the impact locations of bullets 3 and 4 limits the extent of damage in the armor and, consequently, it takes the armor only a slightly longer time to defeat bullet 4 than bullet 3 (39 μs vs. 37 μs). Also, it is clear that since the damage region produced by the impact of bullets 1 and 2 did not extend to the region of impact of the bullets 3 and 4, the times it takes the armor to stop bullets 1,3, and 4 are quite comparable.

An example of the results pertaining to the temporal evolution of the velocities of the four projectiles in the case of the initial bullet velocity of 893 m/s (the highest bullet velocity used in the study of Dolan; Ref 1) is displayed in Fig. 7(b). For each of the four bullets, an "X" is used to denote the moment when the bullet first makes contact with the armor, while a "•" is used to denote the instance of bullet arrest (where applicable). To quantify the multi-hit ballistic performance of the armor in this case, the time periods between the bullet/armor first contact and the bullet arrest (where applicable) or the bullet's exit velocity (where applicable) were recorded for all four bullets as follows: bullet 1—40 μs, bullet 2—247.2 m/s, bullet 3—41.5 μs, and bullet 4—43 μs. The results displayed in Fig. 7(b) clearly show the effect of the multi-hit scenario on the ballistic performance of the transparent armor. Specifically:

(a) While bullet 1 is fully stopped after 40 μs, bullet 2 fully penetrates the armor with a residual velocity of 247.2 m/s;
(b) Since the impact location of bullet 3 is farther away from those of bullets 1 and 2 and the damage induced by bullets 1 and 2 did not extend to the impact location of bullet 3, the armor is successful in stopping bullet 3 and the time to stop bullet 3 is comparable to that for bullet 1.
(c) Since the impact location of bullet 3 is in the vicinity of the right clamped edge of the armor test panel, the resulting damage is apparently not large and widespread to significantly affect the time to stop bullet 4.

### 3.3 Spatial Distribution of Armor Damage

In order to further reveal details regarding the multi-hit ballistic-protection performance of the transparent-armor test-panels studied in the present study, the final spatial distribution of damage in different glass and polycarbonate laminae are recorded and analyzed. An example of the results pertaining to the final spatial distribution of damage within different laminae of the transparent-armor system in the case of the initial bullet velocity of 682 m/s (the highest velocity at which partial penetration of the armor is observed in the study of Dolan; Ref 1) is displayed in Fig. 8(a)-(e). In Fig. 8(a)-(e), five lamina-pairs (each consisting of a glass lamina and the adjacent polycarbonate lamina) are displayed. To improve clarity, glass laminae are assigned a white color, whereas the polycarbonate a cyan color. In Fig. 8(a), the glass lamina corresponds to the transparent-armor strike face, whereas in Fig. 8(e), the polycarbonate lamina corresponds to the armor back-face. An inspection of the results displayed in Fig. 8(a)-(e) reveals that

(a) While the polycarbonate laminae suffer a highly localized damage with a size of the damage region only slightly exceeding the cross-sectional area of the bullet(s), the extent of damage in glass panels is widely spread;
(b) In addition to the damage regions surrounding the points of impact of the four bullets, damage in glass laminae in the regions adjacent to the clamped edges of the test panels are also observed. These peripheral regions of damage are mainly caused by the tensile stress waves reflected off the panel edges and by a higher population of the flaws in the glass laminae at and near their lateral faces;
(c) The role of prior bullet impact(s) in reducing the ballistic protection performance of the transparent-armor and the role of the lateral confinement of the test panels on increasing the ballistic performance can be seen by examining the extent of penetration of the armor by the four bullets. The results of this examination are fully consistent with those displayed in Fig. 8(a). For example, while bullet 1 manages to penetrate only the top-most glass lamina, the tip of bullet 2 is arrested within the third polycarbonate lamina; and
(d) When analyzing the results displayed in Fig. 8(a)-(e), we already know that the material model for glass used in the present study eliminates the finite elements which contain discrete (coarse-fragment) cracks. In other words, glass panel regions containing macro cracks which are commonly observed during testing of the ballistic performance of transparent-armor are removed from the model in the present finite-element formulation. In sharp contrast, finite elements undergoing structural damage because of nucleation of numerous sub-micron cracks are retained in the model. In this way, regions of the glass laminae fractured in the coarse-fragmentation regime and those undergoing a fine-fragmentation failure could be distinguished.

An example of the results pertaining to the final spatial distribution of damage within different laminae of the transparent-armor system in the case of the initial bullet velocity of 893 m/s (the highest bullet velocity used in the study of Dolan; Ref 1) is displayed in Fig. 9(a)-(e). The results displayed in Fig. 9(a)-(e) are quite similar to their corresponding counterparts displayed in Fig. 8(a)-(e) except that the extent of damage is somewhat more widespread and because bullet 2 fully penetrates the test-armor panel.

### 3.4 The Role of Polycarbonate Laminae

As explained earlier, the main role of polycarbonate laminae is to gather the glass fragments and prevent them from entering the interior of the vehicle. Under the standard transient nonlinear dynamics analysis conditions used in the present study, this role of the polycarbonate laminae could not be

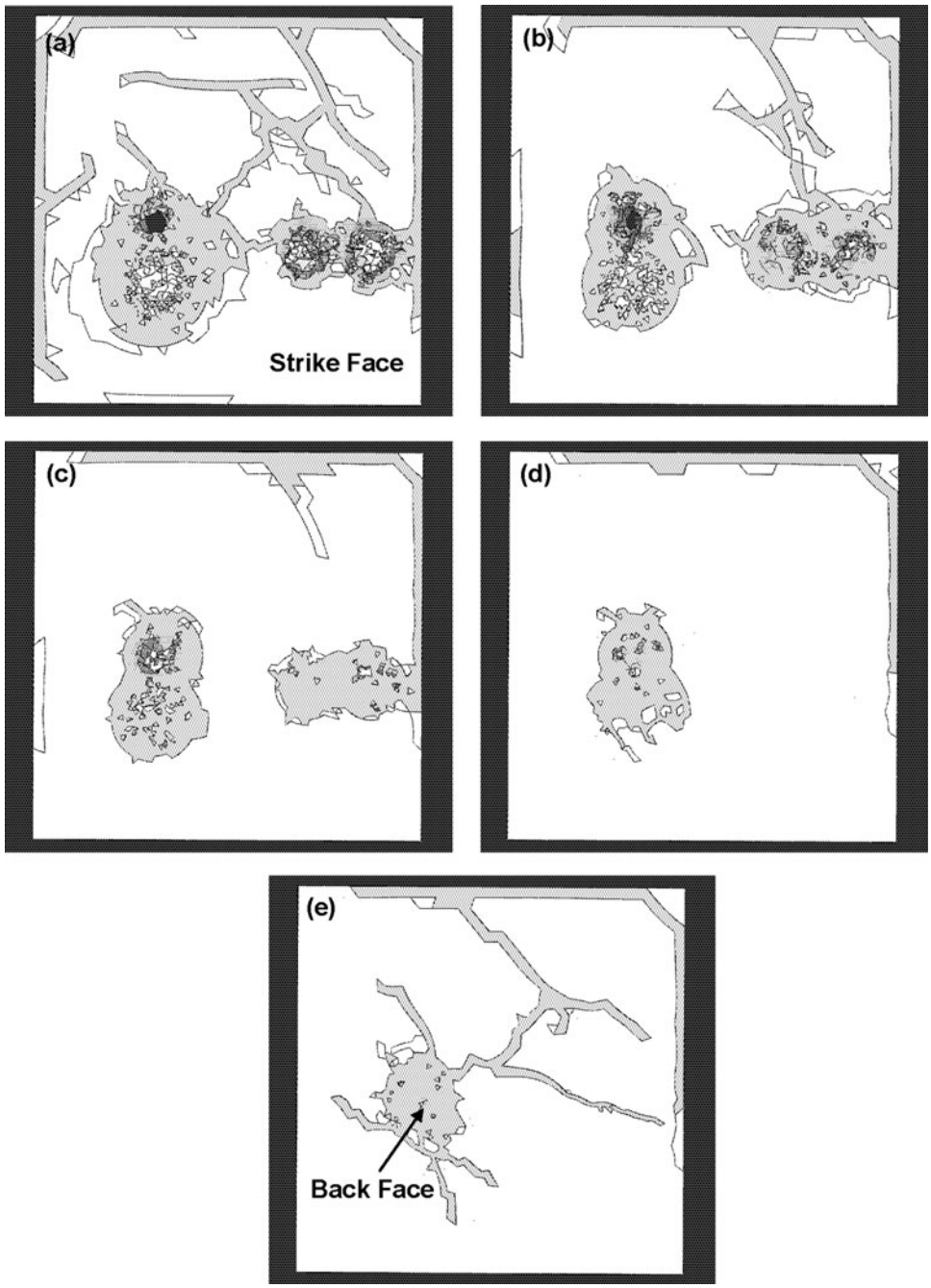


**Fig. 8** Spatial distribution of damage and failure in different glass-polycarbonate lamina pairs for the case of initial projectiles' velocity of 682 m/s

readily revealed (primarily due to the fact that glass-fragments/polycarbonate-laminae interactions were taking place in the interior of the transparent-armor panel). To reveal this role of the polycarbonate laminae, few analyses were carried out under no-interaction conditions between the glass fragments and the polycarbonate laminae. An example of the results obtained in these analyses is displayed in Fig. 10. While under the standard transient nonlinear dynamics analysis conditions used in the present study no glass fragments were observed past the back face of the armor, such fragments are clearly seen in Fig. 10. Thus, the present computational approach is capable of accounting for the role of polycarbonate laminae in gathering the glass fragments.

### 3.5 Transparent-Armor Ballistic-Protection Resistance with Respect to the FSPs

In the initial stage of his experimental investigation, Dolan (Ref 1) carried out a couple of tests dealing with the ballistic-protection performance of the transparent-armor with respect to the 0.50 caliber right circular cylinder steel FSPs. It was found that even at the fragment velocities as low as 592 m/s, the transparent-armor test panels were "*over-matched*" by the FSPs. To further validate the computational procedure used in the present study, few computational analyses dealing with the impact of a 0.50 caliber right circular cylinder steel FSP and the transparent-armor test panel were carried out. The results (not

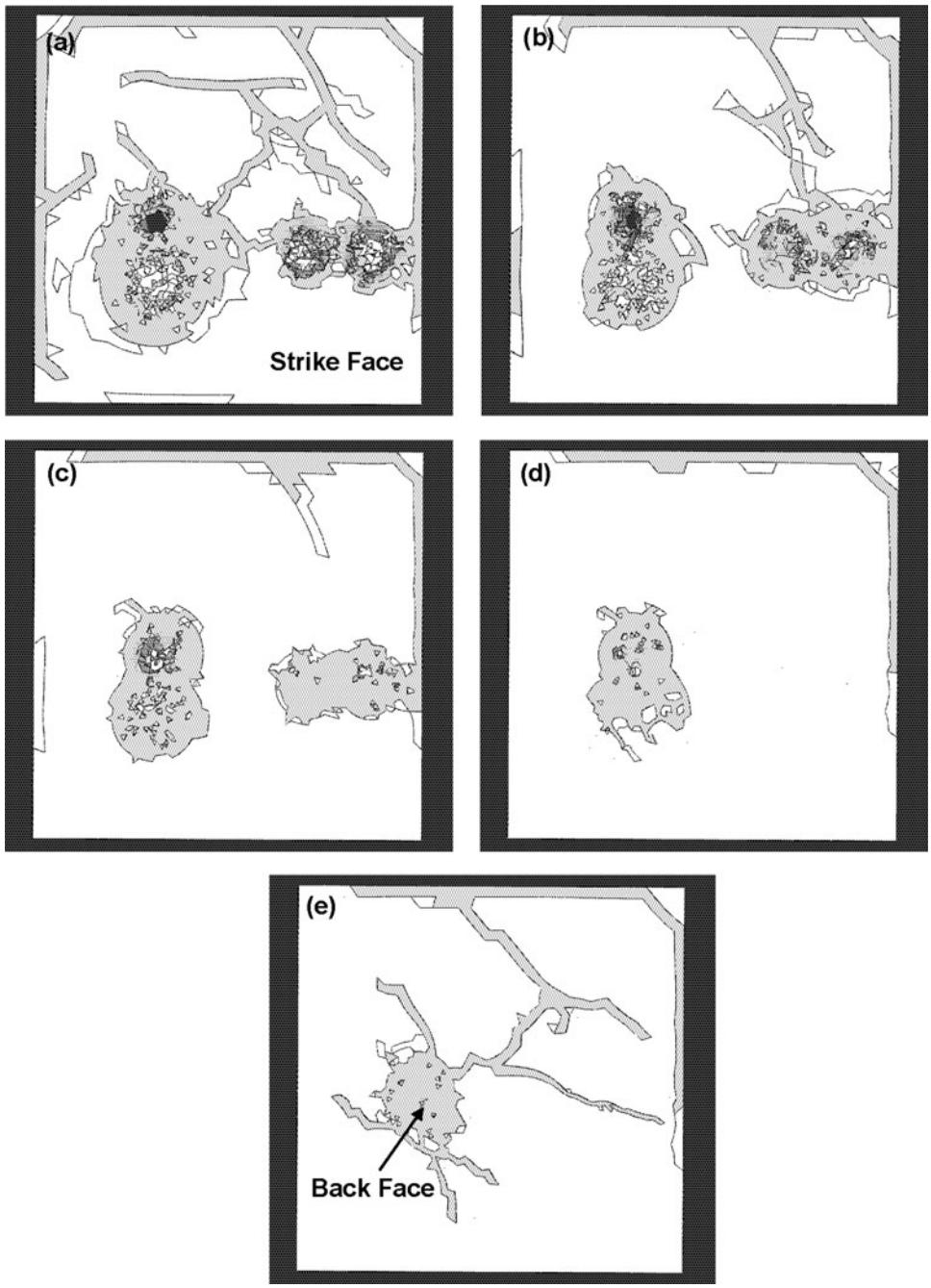


**Fig. 9** Spatial distribution of damage and failure in different glass-polycarbonate lamina pairs for the case of initial projectiles' velocity of 893 m/s

shown for brevity) obtained revealed that indeed the test panels were not able to stop a single FSP at the fragment velocity of 592 m/s. This finding provides additional evidence for physical soundness of the computational method and material models used in the present study.

### *3.6 Future study*

The comparison between the multi-hit ballistic-protection performance computational results and their experimental counterparts obtained in the study of Dolan (Ref 1) for a prototypical laminated glass/polycarbonate transparent-armor system revealed that the computational analyses and the material models used can quite realistically account for the field-test observations. Given this fact, our ongoing study is aimed at extending the present investigation into the area of design optimization to examine how the design parameters, such as the number of glass and polycarbonate laminae, the laminae thicknesses, the grades of these materials, and the bonding strength of the polyurethane adhesive can be selected to further enhance the multi-hit ballistic protection performance of transparent armor.

## 4. Summary and Conclusions

Based on the computational analyses of the multi-hit ballistic-protection performance of laminated transparent-armor

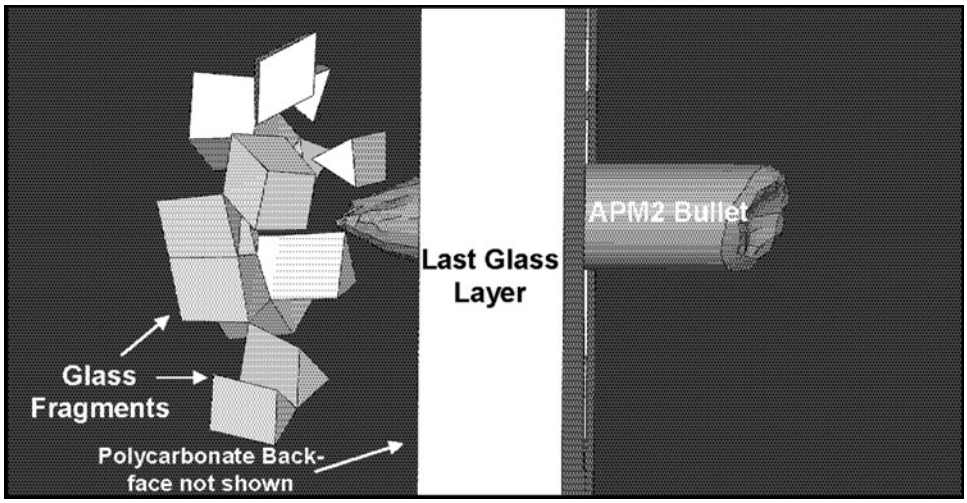


**Fig. 10** When interactions between the glass fragments and the polycarbonate laminae are suppressed, glass fragments can enter the interior of the vehicle

test panels, the following main summary remarks and conclusions can be drawn:

(1) When properly constructed, transient nonlinear dynamics computational analyses offer themselves as a useful tool in understanding the multi-hit ballistic-protection performance of laminated glass/polycarbonate transparent-armor systems.
(2) These analyses can clearly reveal and quantify the extent of loss of the ballistic-protection performance of the armor caused by a sequence of closely spaced bullet impacts.
(3) Through a proper definition of the multi-hit bullet/armor problem and the careful selection of the material models, a reasonably good agreement was obtained between the computational results obtained in the present study and their experimental counterparts obtained by Dolan (Ref 1).
(4) The role of polycarbonate laminae in gathering the glass fragments and preventing them from entering the vehicle interior has also been revealed using the present computational analysis.
(5) The experimentally observed lack of the ballistic protection resistance of the transparent-armor test panels with respect to the 0.50-caliber FSPs is also confirmed computationally.

## References

1. A.M. Dolan, "Ballistic Transparent Armor Testing Using a Multi-Hit Rifle Pattern, Bachelors," Thesis, Kettering University, December 2007
2. ABAQUS Version 6.7, User Documentation, Dessault Systems, 2007
3. M. Grujicic, B. Pandurangan, N. Coutris, B.A. Cheeseman, C. Fountzoulas, P. Patel, and E. Strassburger, A Ballistic Material Model for Starphire®, a Soda-Lime Transparent-Armor Glass, *Mater. Sci. Eng. A*, 2008, **491**(1–2), p 397–411
4. M. Grujicic, B. Pandurangan, W.C. Bell, N. Coutris, B.A. Cheeseman, C. Fountzoulas, and P. Patel, An Improved Mechanical Material Model for Ballistic Soda-Lime Glass, *J. Mater. Eng. Perform.*, 2009, **18**(8), p 1012–1028
5. M. Grujicic, B. Pandurangan, N. Coutris, B.A. Cheeseman, C. Fountzoulas, and P. Patel, A Simple Ballistic Material Model for Soda-Lime Glass, *Int. J. Impact Eng.*, 2009, **36**, p 386–401
6. M. Grujicic, B. Pandurangan, Z. Zhang, W.C. Bell, G.A. Gazonas, P. Patel, and B.A. Cheeseman, Molecular-Level Analysis of Shock-Wave Physics and Derivation of the Hugoniot Relations for Fused Silica, *J. Mater. Eng. Perform.*, 2011, doi:10.1007/s11665-011-0005-2
7. M. Grujicic, W.C. Bell, P.S. Glomski, B. Pandurangan, B.A. Cheeseman, C. Fountzoulas, and P. Patel, Multi-Length Scale Modeling of High-Pressure Induced Phase Transformations In Soda-Lime Glass, *J. Mater. Eng. Perform.*, 2010, doi:10.1007/s11665-010-9774-2
8. M. Grujicic, W.C. Bell, B. Pandurangan, B.A. Cheeseman, C. Fountzoulas, and P. Patel, Molecular-Level Simulations of Shock Generation and Propagation in Soda-lime Glass, *J. Mater. Sci.*, 2011, doi:10.1007/s10853-011-5691-5
9. M. Grujicic, B. Pandurangan, U. Zecevic, K.L. Koudela, and B.A. Cheeseman, Ballistic Performance of Alumina/S-2 Glass-Reinforced Polymer-Matrix Composite Hybrid Lightweight Armor Against Armor Piercing (AP) and Non-AP Projectiles, *Multidiscip. Model. Mater. Struct.*, 2007, **3**, p 287–312
10. E. Strassburger, P. Patel, J.W. McCauley, C. Kovalchick, K.T. Ramesh, and D.W. Templeton, High-Speed transmission Shadowgraphic and Dynamic Photoelasticity Study of Stress Wave and Impact Damage Propagation in Transparent Materials and Laminates Using The Edge-on Impact Method, *Proceedings of the 23rd International Symposium on Ballistics*, Spain, April 2007
11. T. Bjerke, Z. Li, and J. Lambros, Role of Plasticity in Heat Generation during High Rate Deformation and Fracture of Polycarbonate, *Int. J. Plast.*, 2002, **18**, p 549–567
12. A. Needleman, A Continuum Model for Void Nucleation by Inclusion Debonding, *J. Appl. Mech.*, 1987, **54**, p 525–531
13. S. Socrate, "Mechanics of Microvoid Nucleation and Growth in High-Strength Metastable Austenitic Steels," PhD thesis, Massachusetts Institute of Technology, 1995
14. M. Grujicic, V. Sellappan, B. Pandurangan, G. Li, N. Seyr, M. Erdmann, and J. Holzleitner, Computational Analysis of Injection-Molding Residual-Stress Development in Direct-Adhesion Polymer-to-Metal Hybrid Body-In-White Components, *Mater. Process. Technol.*, 2008, **203**(1–3), p 19–36